

## Voltammetric Behavior of a Chemically Modified Silsesquioxane with 4-Amino-5-Phenyl-4h-[1,2,4]-Triazole-3-Thiol and its Application for Detection of L-Dopamine

Daniela Rodrigues Silvestrini, Tayla Fernanda Serantoni da Silveira, Urquiza de Oliveira Bicalho, Devaney Ribeiro Do Carmo\*

Faculdade de Engenharia de Ilha Solteira UNESP - Universidade Estadual Paulista "Júlio de Mesquita Filho" - Departamento de Física e Química, Av. Brasil Centro, 56 – Ilha Solteira, SP, Brasil. CEP. 15.385-000. Fax: +55 (18) 3742-4868.

\*E-mail: [docarmo@dfq.unesp.feis.br](mailto:docarmo@dfq.unesp.feis.br)

Received: 9 December 2014 / Accepted: 24 January 2015 / Published: 24 February 2015

---

A hybrid nanocomposite formed by interaction of a octakis(3-chloropropyl)octasilsesquioxane (SS) modified with 4-Amino-5-Phenyl-4H-1,2,4-Triazole-3-Thiol (APhTT), and its subsequent reaction with copper and hexacyanoferrate (III) (CuHSA) was incorporated into a graphite paste electrode and the electrochemical studies were conducted with cyclic voltammetry. The cyclic voltammogram of the graphite paste electrode modified with CuHSA, showed one redox couple with average potential  $E^{0'} = 0.71\text{V}$  (vs  $\text{Ag}/\text{AgCl}_{(\text{sat.})}$ ), attributed to the  $\text{Cu}^{\text{II}}\text{Fe}^{\text{II}}(\text{CN})_6/\text{Cu}^{\text{II}}\text{Fe}^{\text{III}}(\text{CN})_6$  process (20% w/w;  $v=20\text{ mV s}^{-1}$ ;  $\text{KCl}$ ;  $1.00\text{ mol L}^{-1}$ ). The graphite paste electrode modified with CuHSA allowed the electrocatalytic determination of L-Dopamine using electrochemical techniques such as, cyclic voltammetry and differential pulse voltammetry. Through differential pulse voltammetry was possible to evidence two linear regions in the studied concentration range and the detection limit obtained by this technique was lower than that obtained by the technique of cyclic voltammetry.

---

**Keywords:** Octakis(3-chloropropyl)octasilsesquioxane; 4-Amino-5-Phenyl-4H-[1,2,4]-Triazole-3-Thiol; Voltammetry; Graphite Paste Electrode; L-Dopamine.

### 1. INTRODUCTION

Silsesquioxanes are nanostructured materials which have the empirical formula  $(\text{RSiO}_{1.5})_n$  where R can be a hydrogen or any organic group such as alkyl, methyl, aryl, vinyl, phenyl, arylene or any organofunctional derivative thereof [1-5].

The octahedral cubic silsesquioxanes species (cubes), whose typical structure is  $(\text{RSiO}_{1.5})_8$ , that is, they hold 8 silicon atoms located at the vertices of its structure [3,5-7]. One or more groups (R) can be reactive or polymerizable, which endows the POSS molecule with higher reactivity and solubility in organic solvent.[1] These nanostructured materials have diameters ranging from 1 to 3 nm and are considered the smallest possible silica based particles [2].

Due to the structural similarities and electronic properties exhibited by the silanol groups these materials can mimic the reactivity of silanol groups on the silica surface and these properties are responsible for major advances in understanding the physico-chemical behavior of silsesquioxanes [1,8].

Polysilsesquioxanes are generally synthesized by hydrolytic condensation of the monomer  $\text{RSiX}_3$  [3,8-11] where R is an organic group and X is -Cl, -OH, -OR - $\text{NH}_2$  (alkoxide) or OAc (acetox). The X groups can be hydrolyzed to form Si-OH reactive groups, which can then condense with the formation of bridges Si-O-Si [11,12].

The advantages of using POSS rather than other molecules, such as clays, carbon fibers and carbon nanotubes, is because they are much smaller and have a monodispersed size, low density, and are readily modified chemically to generate a series of reactive substituents to suit a particular application [4]. When organo or inorgano functionalized, silsesquioxanes can improve their chemical and physical properties [2,3,5], for instance, in the adsorption field they can be used to increase the sorptive capacity of metal ions in aqueous or organic solutions [13-15].

The derivatives of POSS can have a hybrid architecture (inorganic/organic) with an internal inorganic structure formed by silicon and oxygen, which is externally covered by organic substituents [16]. These materials are prepared by functionalization reactions in which the organic compound is bonded to the peripheral groups of POSS [17].

The silsesquioxanes have a large number of applications, and the majority of these applications increases when these structures are used as precursors in the formation of organic-inorganic hybrid materials [18, 19].

Such materials exhibit a number of features that permit the your applications in different research areas such as : electronic devices [20], biosensors [2, 4, 5], catalysts [2, 3, 8, 16, 21, 22, 23], electrocatalyst [24,25], electroactive and thin films [26, 27],adsorbents of organic and metal species [28, 29], polymers [2, 4], fuel cells [3], liquid crystals [3, 4], optical fiber coatings [3], additives [3, 30, 31], optical devices [5], antibacterial and biocides [32], core for dendrimers and dendrimers precursors [33] and silica interface precursors [12]. Additionally , cubic silsesquioxanes have its importance in transition metal complexes and also been used in the formations of metal nanoparticles and can form monolayers on gold surfaces [34].

In the last five years, the chemistry of polyhedral silsesquioxane has been extensively reviewed [35-39] and to our knowledge there are relatively few studies which have utilised electrodes chemically modified with silsesquioxane.However are arousing great interest in the area of electrochemistry, due to easy preparation and by possibility of those materials act as power electrocatalysts [40, 41].

In this paper we present the preparation and preliminary characterization of octakis(3-chloropropyl)octasilsesquioxane 4-Amino-5-Phenyl-4*H*-[1,2,4]-Triazole-3-Thiol (APhTT).

Additionally, based on our interest in developing modified electroactive hybrid composites for electroanalytical purposes, was proposed an electroanalytical application of this material. The functionalization of polyhedral oligosilsesquioxane with the 4-Amino-5-Phenyl-4*H*-[1,2,4]-Triazole-3-Thiol, (SA), and respective interactions with  $\text{Cu}^{2+}$  and potassium ferrocyanide (III) following two stages. At the first stage, the SA adsorbs  $\text{Cu}^{2+}$  and in the second step the composite formed (CuSA) reacts with hexacyanoferrate (III) forming a new composite (CuHSA). This ligand possesses S–C–N linkages and displays potential ligands for metal complexes that may also be biologically active just like some other amine- and thione-substituted triazoles [34]. Thus, the interest in using this ligand is due to the fact that it has  $\text{NH}_2$  sites conducive to organofunctionalization with octakis(3-chloropropyl)octasilsesquioxane, as well as S groups that are excellent active sites for the adsorption of metal ions. Thus the S will serve as chelation of  $\text{Cu}^{2+}$  ions.

A synergistic effect can be provide by silsesquioxane. Additionally, the presence of octakis(3-chloropropyl)octasilsesquioxane, which is an electron acceptor [22], can provide stabilizing microenvironment around the substrate. After rigorous voltammetric studies, the composite was tested in the electrocatalytic determination of L-Dopamine which is a neurotransmitter that exists in the mammalian central nervous system [42].

The detection of L-Dopamine was performed using cyclic voltammetry, square wave voltammetry and differential pulse voltammetry.

## 2. EXPERIMENTAL

### 2.1. Reagents and solutions

All reagents and solvents were of analytical grade (Merck or Aldrich) and were used as purchased and L-Dopamine was used without further purification. All solutions and supporting electrolytes were prepared using Milli-Q water. The L-Dopamine solutions were prepared immediately before use.

### 2.2. Electrochemical Measurements

Cyclic voltammograms were performed using the AUTOLAB PGSTAT (Metrohm Pensalab) potentiostat. A three electrodes system was used and it consisted of a modified working electrode (graphite paste electrode), an Ag/AgCl reference electrode and a platinum wire as the auxiliary electrode. The modified paste was prepared by mixing graphite/modifier (CuHSA) in different proportions (10, 20, 30, 40 and 50% (w/w)) and 20  $\mu\text{L}$  of mineral oil (Nujol). It was conducted a preliminary study to select the best ratio of graphite paste. The measurements were carried out at 25°C.

### 2.3. Synthesis of octakis(3-chloropropyl)octasilsesquioxane (SS)

Octakis(3-chloropropyl)octasilsesquioxane (SS) was synthesized following a procedure as described in the literature [43].

800 ml of methanol, 27 ml of hydrochloric acid (HCl) and 43 mL of 3-chloropropyltriethoxysilane were added into a round bottom flask of 1000 mL. The system was kept under constant stirring at room temperature for 6 weeks. The solid phase was separated by filtration in a sintered plate funnel, yielding a white solid, octakis(3-chloropropyl)octasilsesquioxane (SS), which was then oven dried at 120 °C for 4 hours. Figure 1 illustrates a representative scheme of this synthesis.

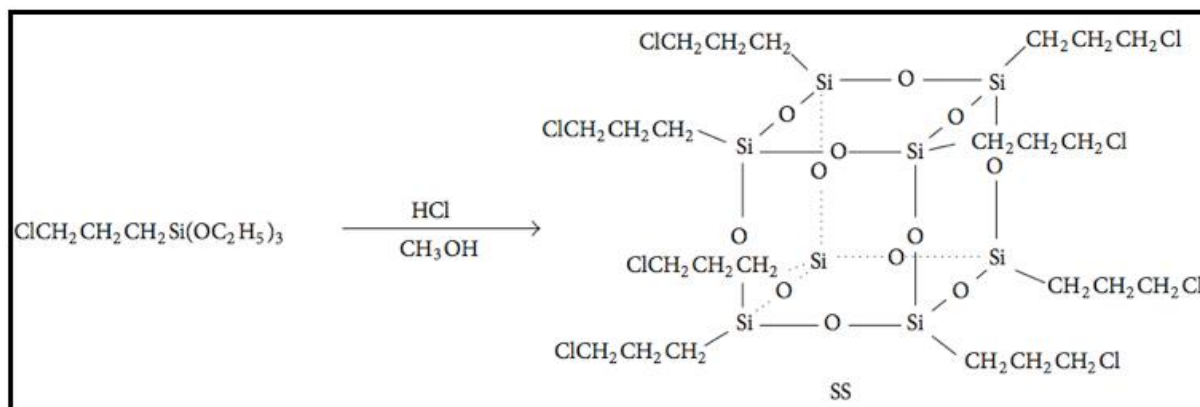


**Figure 1.** Schematic representation of the preparation of octakis(3-chloropropyl)octasilsesquioxane (SS).

#### 2.4. Organofunctionalization of octakis(3-chloropropyl)silsesquioxane with 4-Amino-5-Phenyl-4H-1,2,4-Triazole-3-Thiol (APhTT)

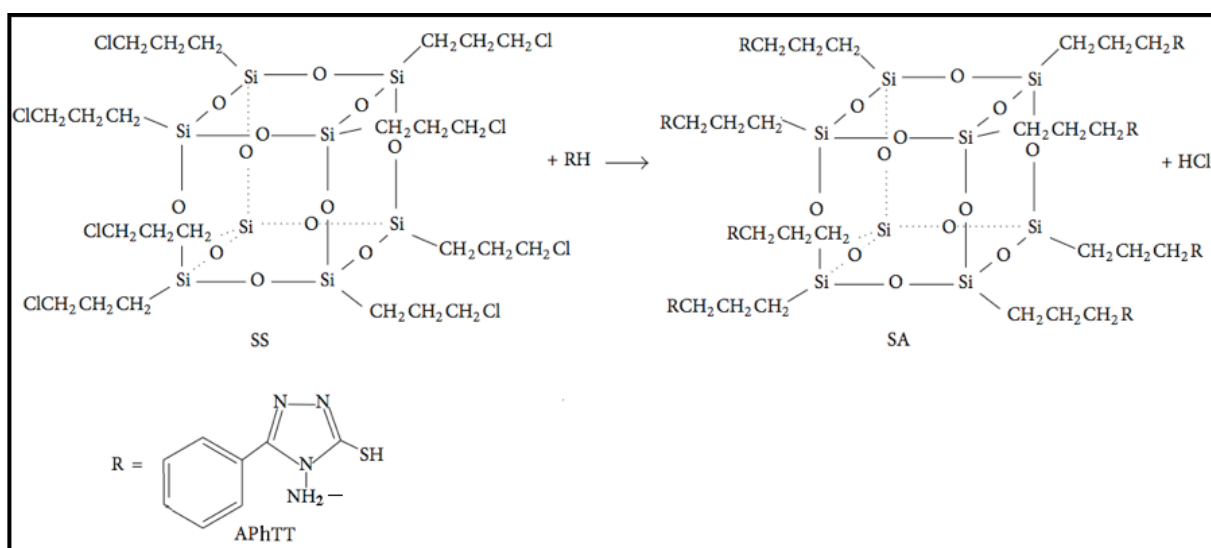


**Figure 2.** Organofunctionalization of octakis(3-chloropropyl)octasilsesquioxane (SS) with APhTT.

Octakis(3-chloropropyl)octasilsesquioxane (SS) was organofunctionalized using a 3-neck flask of 500 mL containing 200 mL of dimethylformamide (DMF),  $9.7 \times 10^{-3}$  of SS, previously dried at 100 °C for 2 hours, and  $8.7 \times 10^{-2}$  mol of 4-Amino-5-Phenyl-4H-1,2,4-Triazole-3-Thiol (APhTT). The

mixture was refluxed at 160°C with constant stirring for 48 hours, then the mixture was precipitated with water due to no formation of solid. After precipitation, the solid plate was separated in a sintered funnel and washed with deionized water. The material obtained was oven dried 100°C for 4 hours and described as SA. Figure 2 schematically illustrates the organofunctionalization process of SS with APhTT.

### 2.5. Formation of complex CuHSA

The CuHSA complexes were prepared as follows: 1.0 g of SA was added to 25 mL of a ketogenic solution of copper chloride  $1.0 \times 10^{-2}$  mol L<sup>-1</sup>. The mixture was stirred for 1h at room temperature. The solid phase was then filtered and washed thoroughly with deionized water. The material resulting from this first phase was designated as CuSA. In the second stage, the CuSA was added to a solution of  $1.0 \times 10^{-2}$  mol L<sup>-1</sup> of potassium hexacyanoferrate (III) and the mixture was stirred for 40 minutes and then the solid was thoroughly filtered, washed with deionized water and dried at 70°C. The material resulting from this stage was described by CuHSA.

### 2.6. Preparation of the graphite paste electrode modified with CuHSA

The graphite paste electrode modified with CuHSA was prepared by mixing 20 mg of CuHSA with 80 mg of graphite and 20  $\mu$ L of mineral oil. The electrode body was produced from a glass tube of 3 mm i.d. and 14 cm height, containing graphite paste. A copper wire was inserted through the opposite end of the glass tube to establish electrical contact. After homogenizing the mixture, the modified paste was carefully positioned on the tube tip to avoid possible air gaps, which often enhances electrode resistance. The external surface of the electrode was smoothed on soft paper. A new surface can be produced by scraping out the old surface and replacing the graphite paste.

### 2.7. Procedure

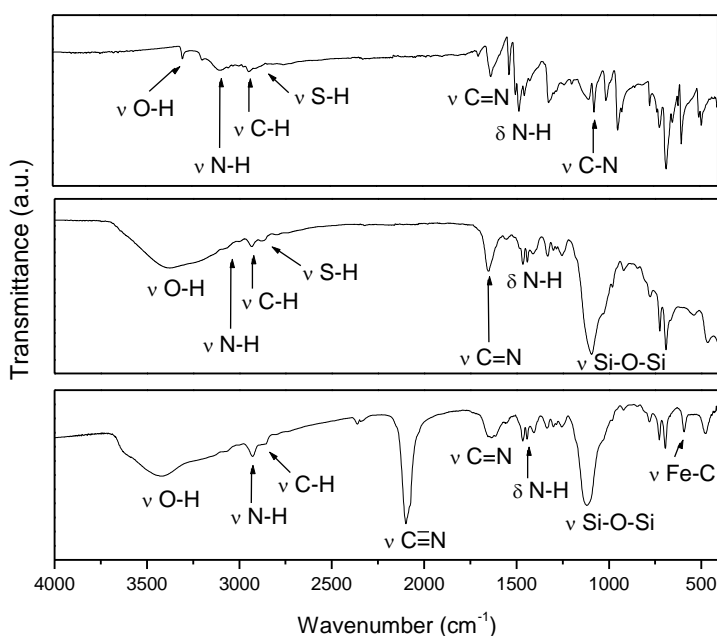
Cyclic voltammograms were recorded for study the sensibility of L-Dopamine by graphite paste electrode modified with CuHSA. The supra analite solutions were prepared immediately before use. In most of the experiments, 1.0 mol L<sup>-1</sup> KCl was used as the supporting electrolyte. The catalytic and or sensibility current was estimated by the difference between the electrode current in the presence of analite compounds and that which is established in the blank solution.

## 3. RESULTS AND DISCUSSION

Figure 3 (A) and (B) illustrate the vibrational spectra of 4-Amino-5-Phenyl-4H-1,2,4-Triazole-3-Thiol (APhTT) and functionalized material (SA), respectively. In the spectrum shown by SA was observed characteristic absorption bands of the precursor materials. The band observed at about 1082

$\text{cm}^{-1}$  is related to the stretching  $\text{Si-O-Si}_{(\nu\text{Si-O-Si})}$  corresponding to the cage-shaped structure of silsesquioxane showing that the cubic structure of matrix was maintained. Other bands were observed in the region of  $2900 \text{ cm}^{-1}$  assigned to the axial deformation of the  $\text{C-H}_{(\delta\text{C-H})}$  bonds, present on both precursors. The band at  $3079 \text{ cm}^{-1}$  was assigned to the axial deformation of  $\text{N-H}_{(\delta\text{N-H})}$  and about at  $2870 \text{ cm}^{-1}$  was attributed to axial deformation of  $\text{S-H}_{(\delta\text{S-H})}$  [44, 45]. The bands from  $500$  to  $1600 \text{ cm}^{-1}$  were related to the vibrations of the axial deformation of the ring bonds of APhTT. Also observed a decrease of absorption about at  $689 \text{ cm}^{-1}$  related to the vibrations  $\text{C-Cl}$  of the SS, thus showing its functionalization and suggesting that not all peripheral groups reacted with the ligand 4-Amino-5-Phenyl-4*H*-1,2,4-Triazole-3-Thiol.

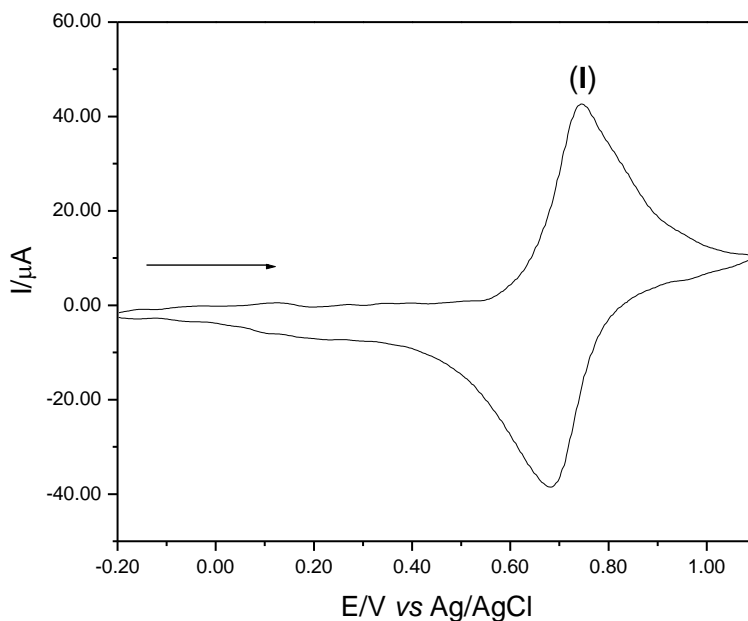
Figure 3 (C) shows the spectrum in the infrared region for the modified material CuHSA. The spectrum shows typical vibrations of its precursor materials at  $\sim 1110 \text{ cm}^{-1}$  for the asymmetric stretching  $\text{Si-O-Si}_{(\nu\text{Si-O-Si})}$  which corresponds to the cage shaped structure of silsesquioxane. The bands at  $\sim 2930 \text{ cm}^{-1}$  was attributed to the vibration of  $\text{C-H}_{(\nu\text{C-H})}$  bonds and from  $2870$  to  $2930 \text{ cm}^{-1}$  was attributed to axial deformation of  $\text{S-H}_{(\delta\text{S-H})}$ . The vibrations from  $1200$  to  $1600 \text{ cm}^{-1}$  was related to the vibrations of the APhTT ring. It was also observed vibrations at  $\sim 2100 \text{ cm}^{-1}$ , which was attributed to  $\text{C}\equiv\text{N}_{(\nu\text{C}\equiv\text{N})}$  stretching, characteristic of the transition metal hexacyanoferrate, where in the nanocomposite (CuHSA) the  $\nu\text{C}\equiv\text{N}$  is displaced about  $64 \text{ cm}^{-1}$  for higher frequencies (high energy) relative to the potassium hexacyanoferrate (III), which is one indicative of the formation of the intervalence complex where  $\text{CN}^-$  is connected to the metal centers  $\text{Fe}^{\text{III}}-(\text{CN})-\text{Cu}^{\text{II}}$  [46]. Additionally, it was possible to observe a vibration at  $594 \text{ cm}^{-1}$  related to the stretching  $\text{Fe-C}_{(\nu\text{Fe-C})}$  [47].



**Figure 3.** Vibrational spectra in the infrared region: (A) APhTT, (B) SA and (C) CuHSA.

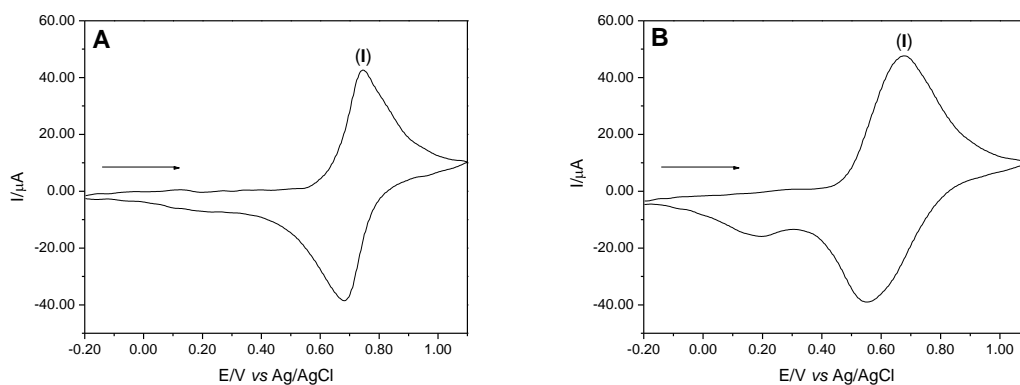
In order to investigate the presence of the metal complex formed with the CuHSA, there was a detailed study on the voltammetric behavior of the prepared materials. Figure 4 illustrates the cyclic

voltammogram of graphite paste modified with CuHSA (20% w/w). The voltammogram of CuHSA showed only a redox pair,  $E^{\theta} = 0.71$  V, assigned to  $\text{Cu}^{\text{II}}\text{Fe}^{\text{II}}(\text{CN})_6/\text{Cu}^{\text{II}}\text{Fe}^{\text{III}}(\text{CN})_6$ .



**Figure 4.** Cyclic voltammogram of graphite paste modified with CuHSA (20% w/w;  $\nu = 20 \text{ mV s}^{-1}$ ; KCl;  $1.00 \text{ mol L}^{-1}$ ).

Figure 5 illustrates the studies carried out on different supporting electrolytes, such as KCl, NaCl, LiCl,  $\text{KNO}_3$  and  $\text{NaNO}_3$ . It was observed that the nature of the cations and anions affected the average potential ( $E^{\theta}$ ) and the current intensities, as shown in Table 1. In addition, these studies indicate that there was formation of a crystal lattice to CuHSA system. The CuHSA is a compound analogous to Prussian blue and it exhibits a zeolite structure type, showing cavities that allow the inflow and outflow of some alkaline metal ions with smaller hydration radii [48-50].



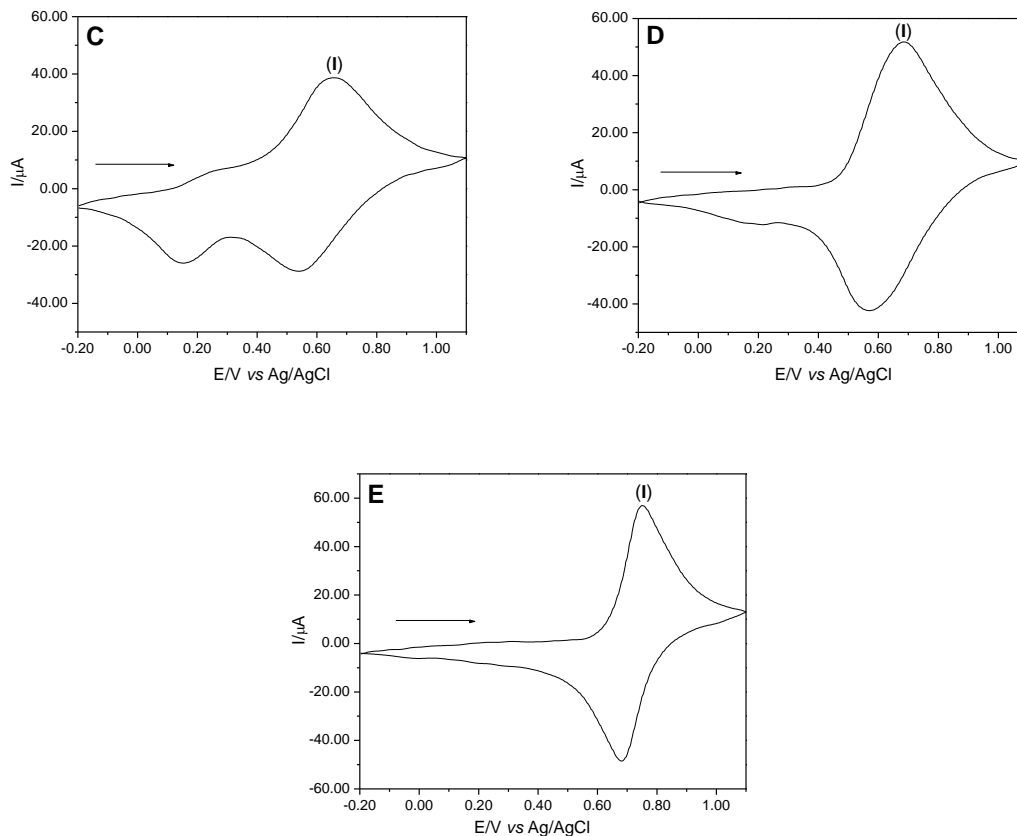


**Figure 5.** Cyclic voltammograms of graphite electrode modified with CuHSA in different supporting electrolytes: (A) KCl, (B) NaCl, (C) LiCl, (D) NaNO<sub>3</sub> and (E) KNO<sub>3</sub> (20% (w/w),  $\nu = 20 \text{ mV s}^{-1}$ ,  $1.00 \text{ mol L}^{-1}$ ).

The ratio  $I_{pa}/I_{pc}$  and  $\Delta E_p$  were of  $\sim 1.00$  to  $1.26$  and from  $0.06$  to  $0.12$ , respectively, for the different supporting electrolytes tested, which suggests that the process  $\text{Cu}^{\text{II}}\text{Fe}^{\text{II}}(\text{CN})_6/\text{Cu}^{\text{II}}\text{Fe}^{\text{III}}(\text{CN})_6$  is quasi reversible.

**Table 1.** Electrochemical parameters of the graphite paste modified with CuHSA in different supporting electrolytes (20% w/w,  $\nu = 20 \text{ mV s}^{-1}$ ,  $1.00 \text{ mol L}^{-1}$ ).

Supporting electrolyte	$I_{pa}$ ( $\mu\text{A}$ )	$I_{pc}$ ( $\mu\text{A}$ )	$ I_{pa}/I_{pc} $	$E_{pa}$ (V)	$E_{pc}$ (V)	$\Delta E_p$ (V)	$E^0$ (V)	Diameter of the hydrated cation (nm)**
KCl	$3.81 \times 10^{-5}$	$3.81 \times 10^{-5}$	1.00	0.74	0.68	0.06	0.71	0.24
NaCl	$4.42 \times 10^{-5}$	$3.50 \times 10^{-5}$	1.26	0.68	0.56	0.12	0.61	0.36
LiCl	$2.20 \times 10^{-5}$	$1.76 \times 10^{-5}$	1.25	0.65	0.55	0.10	0.60	0.47
NaNO <sub>3</sub>	$4.72 \times 10^{-5}$	$3.83 \times 10^{-5}$	1.23	0.68	0.57	0.11	0.62	0.36
KNO <sub>3</sub>	$5.02 \times 10^{-5}$	$4.56 \times 10^{-5}$	1.10	0.75	0.68	0.07	0.71	0.24

\*\*[48]



It was observed that the voltammetric behavior of the CuHSA is different for all electrolytes tested due mainly to the diameter of the hydrated radius of the cation. The process of oxidation and reduction of compounds modified at the surface CuHSA occurs initially through equilibrium of the cation present in the supporting electrolyte with electrode surface containing material. The cation  $K^+$  and  $NH_4^+$  have smaller hydration radii and therefore can more easily penetrate the crystal lattice characteristic of the binuclear complex [48]. For subsequent voltammetric studies, KCl was used as supporting electrolyte, because it presented a better performance and voltammetric parameters.

Figure 6 illustrates the cyclic voltammograms of graphite paste modified with CuHSA in different KCl concentrations ( $0.10$ - $2.00 \text{ mol L}^{-1}$ ). It was observed that the performance becomes different and there is an increase in the current intensity with increasing concentration of the supporting electrolyte. Through this study, it was observed that for the graphite paste electrode modified with CuHSA, the line slope was of  $51.5 \text{ mV}$  per decade of potassium ions (Figure 7), indicating that the behavior exhibited by the electrode approaches a nerstian process with transfer of an electron [51, 52].

It was also found that the relationship between the average potential and the logarithm ( $\log$ ) of the  $K^+$  concentration of the redox pair showed a linear relationship, as shown in Figure 7, making clear that the redox process is highly dependent on the concentration of  $K^+$ .

After this study, the concentration of the supporting electrolyte chosen to continue the ensuing studies was  $1.00 \text{ mol L}^{-1}$  due to the better voltammetric performance.

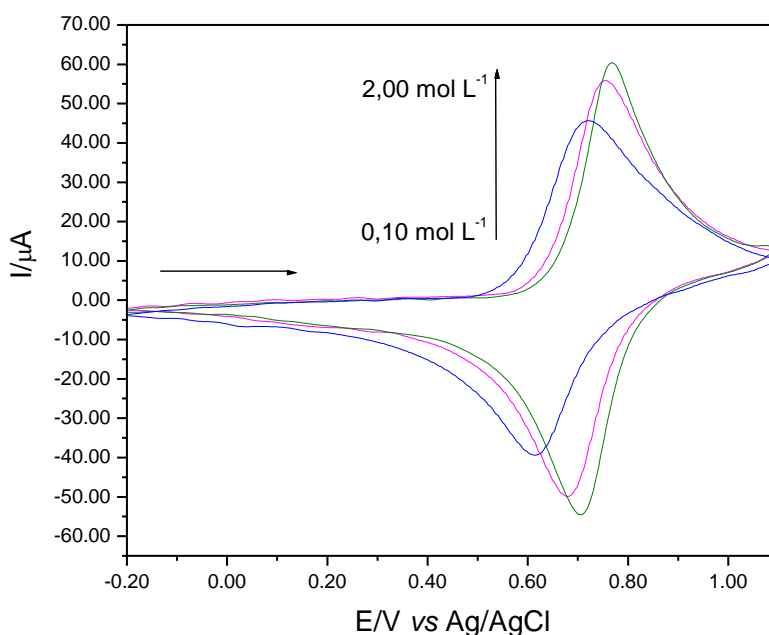


**Figure 6.** Cyclic voltammograms of graphite electrode modified with CuHSA in different supporting electrolyte concentrations (20% (w/w),  $\nu = 20 \text{ mV s}^{-1}$ ).

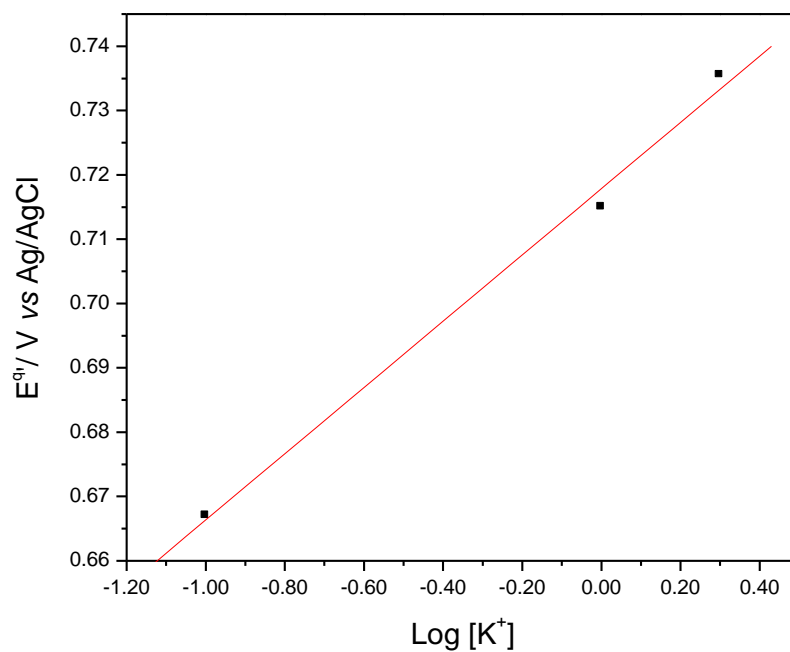


**Figure 7.** Average potential ( $E^0$ ) of graphite paste modified with CuHSA as a function of KCl concentration.

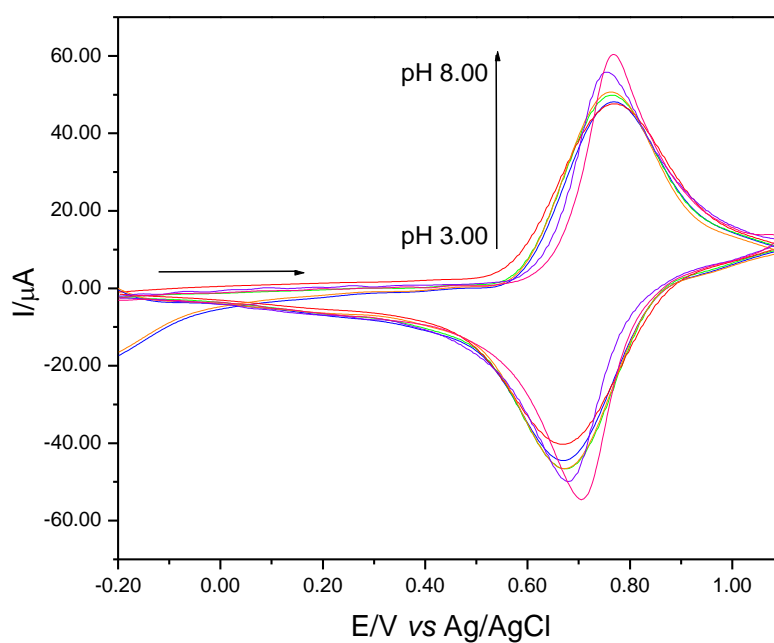


**Figure 8.** Cyclic voltammograms of the graphite paste modified with CuHSA at different pH values (3.0 to 8.0); (20% w/w,  $\nu = 20\text{mV s}^{-1}$ , KCl  $1.0\text{ mol L}^{-1}$ ).

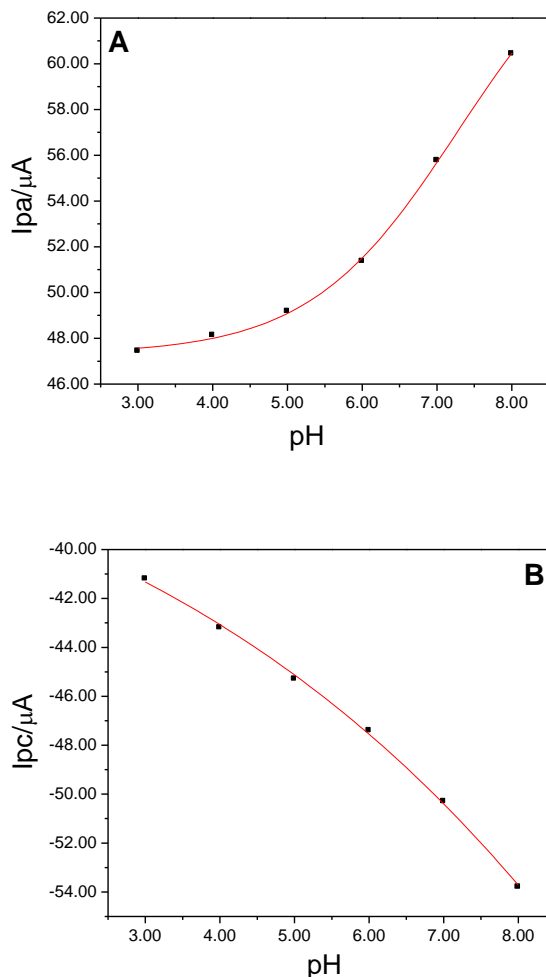


**Figure 9.** (A) Anodic current intensity ( $I_{pa}$ ) and (B) cathodic current intensity ( $I_{pc}$ ) as function of pH values (3.0 to 8.0) (20% w/w,  $\nu = 20\text{mV s}^{-1}$ , KCl  $1.0\text{ mol L}^{-1}$ ).

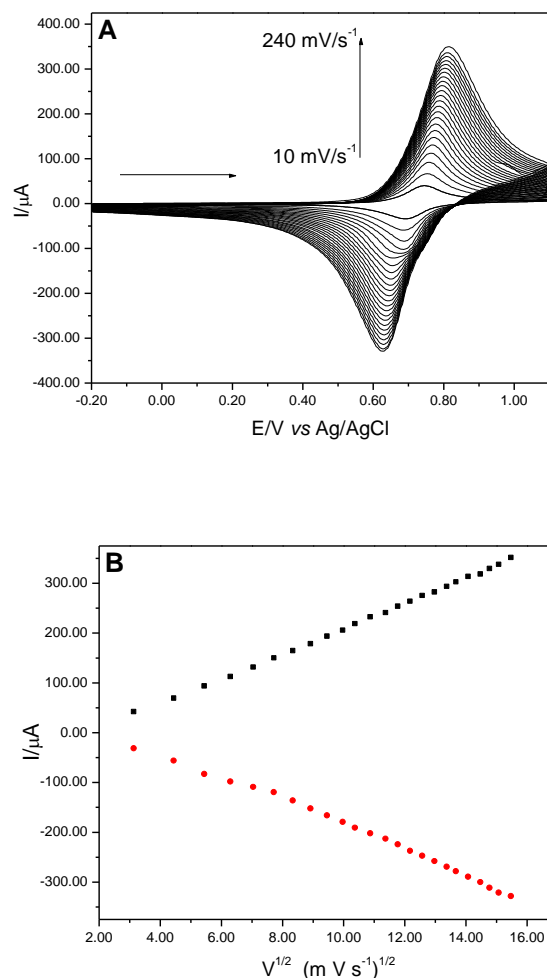
The cyclic voltammograms at different hydrogen ion concentrations (pH 3.0 to 8.0) obtained for CuHSA are illustrated in Figure 8. It was found that with the pH increase there is a increase in the current intensity. The  $E^{\theta'}$  remained constant about at 0.71 V. The current intensity is greater at higher pH due to the concentration of  $\text{H}^+$  ions, and these compete with  $\text{K}^+$  ions in the redox process.

Figure 9 illustrates the dependence of anodic and cathodic current intensity at different pH values for CuHSA. Through these graphs, it is observed that at pH between 3.00 to 5.00 the anodic current remains practically constant (ranging  $\sim 2.00\text{ uA}$ ). For cathodic current occurs a variation of  $\sim 6.00\text{ uA}$ , but to  $\text{pH} \geq 6.00$  is much higher intensity of anodic current ( $\sim 10.47\text{ uA}$ ) and also the cathodic current intensity ( $\sim 6.00\text{ uA}$ ).

The pH value chosen for further studies was pH 7.00, since there is the possibility of conducting studies to determination electrocatalytic of drugs in a biological environment.

Figure 10 (A) illustrates the CuHSA voltammetric behavior of the system at different scan rates ( $10\text{-}240\text{ mV s}^{-1}$ ). It was observed that there is an increase of current intensity with an increase of the

system scan rate and average potential ( $E^{\theta}$ ) remained constant at 0.71 V. It was observed that the scan rate increase provides an increase in the resistance, causing an increase in  $\Delta E_p$  at higher scan rates. The linear dependence of the current intensity of the anodic/cathodic peak and the square root of scan rate (Figure 10 (B)) characterizes a diffusion process [51].



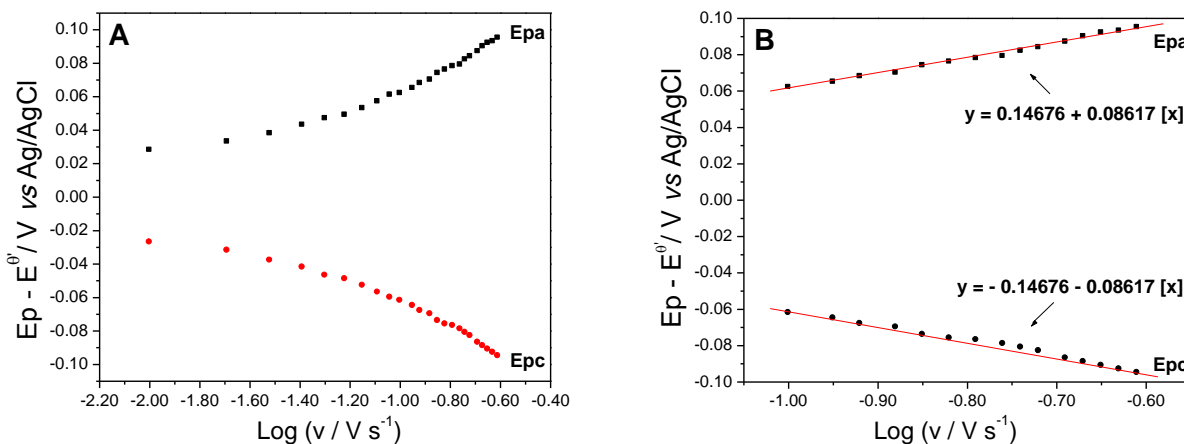
**Figure 10.** (A) Cyclic voltammograms of the graphite paste modified with CuHSA at different scan rates (10-240  $\text{mV s}^{-1}$ ) (20% w/w, KCl 1.0  $\text{mol L}^{-1}$ , pH 7.00). (B) Dependence on current intensity of the anodic and cathodic peaks with the square root of the scan rate.

Figure 11 shows the Laviron's graphic, where it is noted that the potential difference between the anodic ( $E_{pa}$ ) and cathodic ( $E_{pc}$ ) peaks and the formal potential ( $E_p - E^{\theta}$ ) is dependent on the potential scan rate. The Laviron's equation can be applied to high and low scan rates,  $\Delta E_p > 200 \text{ n/mV}$  and  $\Delta E_p < 200 \text{ n/mV}$ , respectively [53].

From the derived equations of Laviron's equation (Equation 1), it is possible to determine the transfer coefficient ( $\alpha$ ) - by measuring the variation of the potential of anodic and cathodic peaks vs. the log of the scan rate ( $\nu$ ) as well as the charge transfer constant ( $ks$ ) - to transference of electrons between the electrode and the surface layer. According to Laviron's equation,  $E_p - E^{\theta}$  vs.  $\log \nu$

produces two lines with slope  $2.3RT/(1-\alpha)nF$  to anodic peak and  $-2.3RT/\alpha nF$  to cathodic peak [54, 55].

$$\text{Log } ks = \alpha \text{log}(1-\alpha) + (1-\alpha) \text{log } \alpha - \text{log } \frac{RT}{nFv} - \frac{\alpha nF(1-\alpha)}{2,3RT} \frac{\Delta E_p}{2,3RT} \tag{Eq. 1}$$



**Figure 11.** (A) Laviron’s graphic, Epa and Epc vs. Log v. (B) Equation of the straight line of Laviron’s graphic, Epa and Epc vs. Log v.

Table 2 shows the electrochemical parameters used in making the Laviron’s graphic.

**Table 2.** Electrochemical parameters used in making the Laviron’s graphic.

Log of the scan rate ( $V s^{-1}$ )	Epa - $E^\theta$ (V)	Epc - $E^\theta$ (V)
-2.00	0.028	-0.027
-1.69	0.033	-0.032
-1.52	0.038	-0.038
-1.39	0.043	-0.042
-1.30	0.047	-0.047
-1.22	0.049	-0.049
-1.15	0.053	-0.053
-1.09	0.057	-0.057
-1.04	0.061	-0.060
-1.00	0.062	-0.062
-0.95	0.065	-0.065
-0.92	0.068	-0.068
-0.88	0.070	-0.070
-0.85	0.074	-0.074
-0.82	0.076	-0.076
-0.79	0.078	-0.077
-0.76	0.079	-0.079

-0.74	0.082	-0.081
-0.72	0.084	-0.083
-0.69	0.087	-0.087
-0.67	0.090	-0.089
-0.65	0.092	-0.091
-0.63	0.093	-0.093
-0.61	0.095	-0.095

Assuming that an electron be involved in the redox process, and that  $\alpha$  is equal to 0.315 and 0.685 for the anodic and cathodic peaks, respectively. The calculated value for  $k_s$  was of  $0.65 \text{ s}^{-1}$ .

### 3.1. Electrocatalytic oxidation of L-Dopamine by cyclic voltammetry

The electrocatalytic oxidation of L-Dopamine in the graphite paste electrode modified with CuHSA is illustrated in Figure 12, where it was observed that the graphite paste electrode unmodified in the absence of L-Dopamine (A) didn't show any redox pair in the potential range between -0.2 and 1.1 V, however, in the presence of L-Dopamine (B), it was possible to observe the redox process of the L-Dopamine with  $E^{0'} = 0.39 \text{ V}$ . The graphite paste electrode modified with CuHSA in the absence of L-Dopamine (C) exhibited a redox pair with  $E^{0'} = 0.71 \text{ V}$ , however, in the presence of L-Dopamine (D), there was an increase in anodic peak current intensity of the redox pair, followed by a slight increase in cathodic peak current intensity.

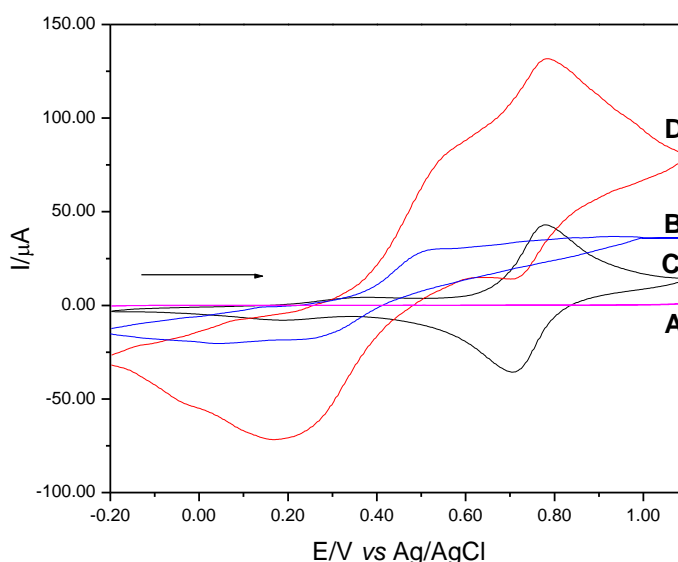
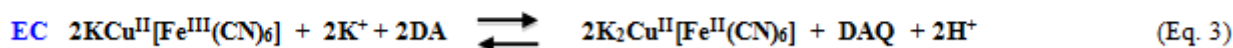
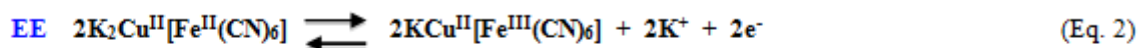


**Figure 12.** Cyclic voltammograms of: (A) graphite paste electrode unmodified in the absence of L-Dopamine, (B) graphite paste electrode unmodified in presence of  $4.00 \times 10^{-3} \text{ mol L}^{-1}$  of L-Dopamine, (C) graphite paste electrode modified with CuHSA in the absence of L-Dopamine and (D) graphite paste modified with CuHSA in presence of  $4.00 \times 10^{-3} \text{ mol L}^{-1}$  of L-Dopamine.

The anodic peak current intensity increases due to the electrocatalytic oxidation of L-Dopamine. The  $\text{Fe}^{\text{III}}$  produced during the anodic scan, chemically oxidizes the L-Dopamine, whereas  $\text{Fe}^{\text{III}}$  is reduced to  $\text{Fe}^{\text{II}}$  is reduced, which will again be electrochemically oxidized to  $\text{Fe}^{\text{III}}$  [56]. The electrochemical and chemical stages of the system are represented by equations 2 and 3, respectively [57, 58].



Where: DA = L-Dopamine and DAQ = Product of L-Dopamine oxidation (Dopamine-quinone) [59].

Figure 13 shows the voltammetric behavior of the system CuHSA after the additions of different aliquots of L-Dopamine. The analytic curve, showing the anodic current as a function of L-Dopamine concentration for CuHSA is illustrated in Figure 14. The modified graphite paste electrode showed a linear response in the concentration range of  $9.00 \times 10^{-4}$  to  $4.00 \times 10^{-3}$  mol L<sup>-1</sup>, presented a corresponding equation  $Y \text{ (A)} = 1.69 \times 10^{-6} + 0.022 [\text{L-Dopamine}]$  and a correlation coefficient  $r^2 = 0.999$ . The detection limit obtained for this system was of  $2.08 \times 10^{-4}$  mol L<sup>-1</sup> with a relative standard deviation of  $\pm 2\%$  ( $n = 3$ ) and an amperometric sensitivity of 0.022 A/mol L<sup>-1</sup>.

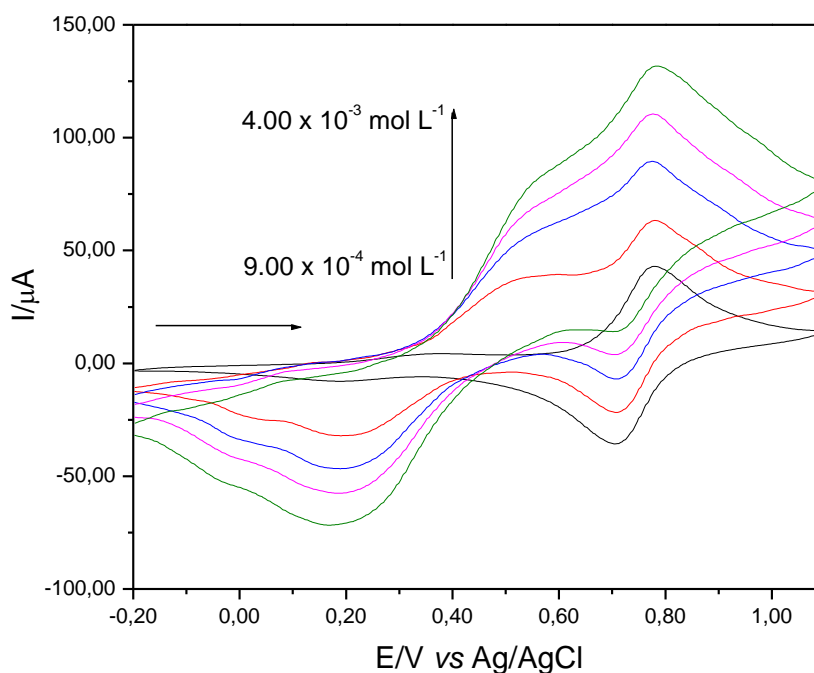


**Figure 13.** Cyclic voltammograms obtained for the graphite paste electrode modified with CuHSA in the presence of different L-Dopamine concentrations ( $9.00 \times 10^{-4}$  to  $4.00 \times 10^{-4}$  mol L<sup>-1</sup>); (20% w/w,  $\nu = 20$  mV s<sup>-1</sup>, KCl, 1.00 mol L<sup>-1</sup>, pH 7.00).

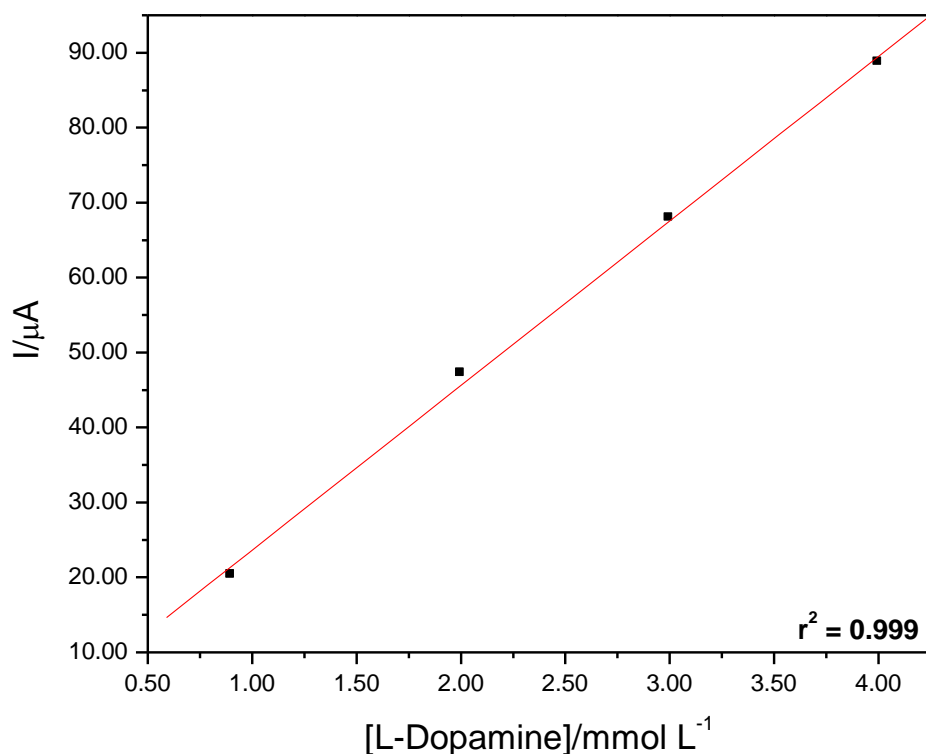


**Figure 14.** Analytic curve of the anodic peak current as a function of L-Dopamine concentration using the graphite paste electrode modified with CuHSA (20% w/w,  $v = 20 \text{ mV s}^{-1}$ , KCl,  $1.00 \text{ mol L}^{-1}$ , pH 7.00).

### 3.2. Electrocatalytic oxidation of L-Dopamine by differential pulse

For the system (CuHSA) was also tested the differential pulse voltammetry technique (DPV). Figure 15 illustrates the behavior of the DPV of the CuHSA after the additions of different aliquots of L-Dopamine.

Through differential pulse voltammetry was possible to evidence two linear regions of the studied concentration range which are illustrated in Figure 16 (A) and (B). The analytical curves, showing the anodic current versus concentration of L-Dopamine for CuHSA system can be observed in Figure 17. The first region showed a linear response in the concentration range of  $5.00 \times 10^{-5}$  to  $1.00 \times 10^{-4} \text{ mol L}^{-1}$  with a corresponding equation  $Y(\text{A}) = 6.51 + 1.386 \times 10^{-5} [\text{L-Dopamine}]$  and a correlation coefficient  $r^2 = 0.999$ . The detection limit was of  $1.70 \times 10^{-4} \text{ mol L}^{-1}$  with a relative standard deviation of  $\pm 4\%$  ( $n = 3$ ) and amperometric sensitivity of  $1.385 \text{ A/mol L}^{-1}$ . The second region showed a linear response in the concentration range of  $1.00 \times 10^{-4}$  to  $8.00 \times 10^{-4} \text{ mol L}^{-1}$  with a corresponding equation  $Y(\text{uA}) = 6.22 \times 10^{-5} + 0.9906 [\text{L-Dopamine}]$  and a correlation coefficient  $r^2 = 0.998$ . The detection limit was of  $5.27 \times 10^{-5} \text{ mol L}^{-1}$  with a relative standard deviation of  $\pm 2\%$  ( $n = 3$ ).



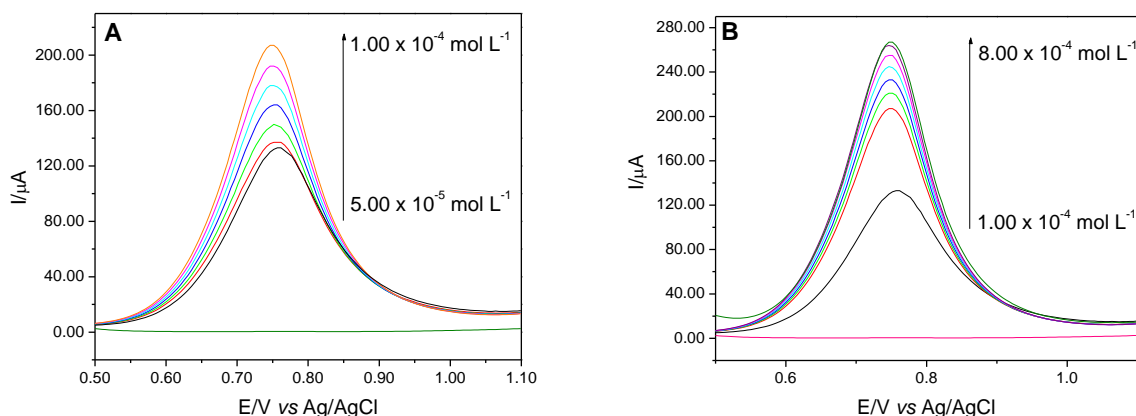


**Figure 15.** Differential pulse voltammograms obtained for the graphite paste electrode modified with CuHSA in the presence of different L-Dopamine concentrations (20% w/w,  $\nu = 10 \text{ mV s}^{-1}$ , KCl,  $1.00 \text{ mol L}^{-1}$ , pH 7.00, pulse amplitude of 50 mV). (A)  $5.00 \times 10^{-5}$  to  $1.00 \times 10^{-4} \text{ mol L}^{-1}$ , (B)  $1.00 \times 10^{-4}$  to  $8.00 \times 10^{-4} \text{ mol L}^{-1}$ .

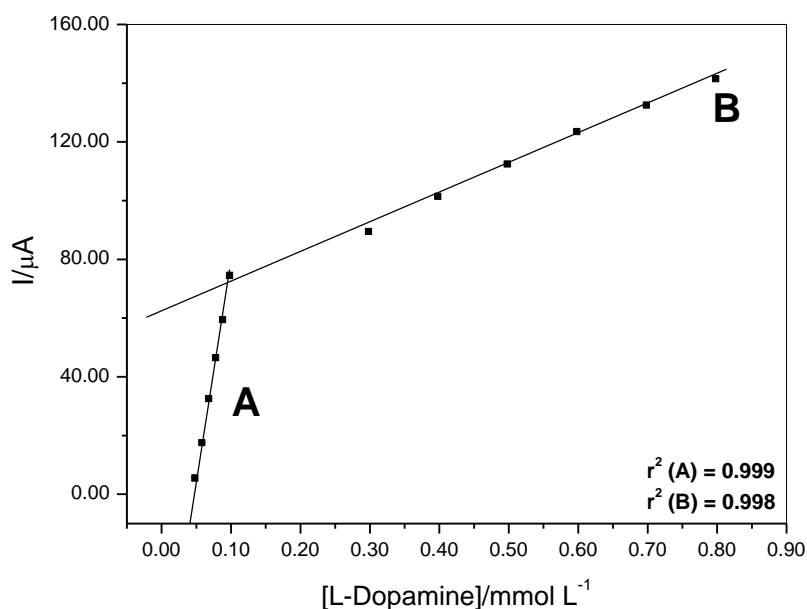


**Figure 16.** Analytic curve determined for CuHSA for determination of L-Dopamine in two concentration ranges: (A)  $5.00 \times 10^{-5}$  to  $1.00 \times 10^{-4} \text{ mol L}^{-1}$ , (B)  $1.00 \times 10^{-4}$  to  $8.00 \times 10^{-4} \text{ mol L}^{-1}$ .

#### 4. CONCLUSION

The voltammetric behavior of CuHSA presented a redox couple well defined with  $E^0 = 0.71 \text{ V}$ , assigned to  $\text{Cu}^{\text{II}}\text{Fe}^{\text{II}}(\text{CN})_6/\text{Cu}^{\text{II}}\text{Fe}^{\text{III}}(\text{CN})_6$  (20% w/w;  $\nu = 20 \text{ mV s}^{-1}$ ; KCl;  $1.00 \text{ mol L}^{-1}$ ). The graphite paste electrode modified with CuHSA allowed the electrocatalytic determination of L-dopamine using two electrochemical techniques such as, cyclic voltammetry and differential pulse voltammetry. The

modified graphite paste electrode showed a linear response in the concentration range of  $9.00 \times 10^{-4}$  to  $4.00 \times 10^{-3}$  mol L<sup>-1</sup>, presented a corresponding equation  $Y(A) = 1.69 \times 10^{-6} + 0.022 [\text{L-Dopamine}]$  and a correlation coefficient  $r^2 = 0.999$ . The detection limit obtained for this system using the cyclic voltammetry technique was of  $2.08 \times 10^{-4}$  mol L<sup>-1</sup> with a relative standard deviation of  $\pm 2\%$  ( $n = 3$ ) and an amperometric sensitivity of  $0.022 \text{ A/mol L}^{-1}$ . Through differential pulse voltammetry was possible to evidence two linear regions of the studied concentration range. The analytical curves, showing the anodic current versus concentration of L-Dopamine for CuHSA system can be observed in Figure 17. The first region showed a linear response in the concentration range of  $5.00 \times 10^{-5}$  to  $1.00 \times 10^{-4}$  mol L<sup>-1</sup> with a corresponding equation  $Y(A) = 6.51 + 1.386 \times 10^{-5} [\text{L-Dopamine}]$  and a correlation coefficient  $r^2 = 0.999$ . The detection limit was of  $1.70 \times 10^{-4}$  mol L<sup>-1</sup> with a relative standard deviation of  $\pm 4\%$  ( $n = 3$ ) and amperometric sensitivity of  $1.385 \text{ A/mol L}^{-1}$ . The second region showed a linear response in the concentration range of  $1.00 \times 10^{-4}$  to  $8.00 \times 10^{-4}$  mol L<sup>-1</sup> with a corresponding equation  $Y(\mu\text{A}) = 6.22 \times 10^{-5} + 0.9906 [\text{L-Dopamine}]$  and a correlation coefficient  $r^2 = 0.998$ . The detection limit was of  $5.27 \times 10^{-5}$  mol L<sup>-1</sup> with a relative standard deviation of  $\pm 2\%$  ( $n = 3$ ). Thus, the composite CuHSA is a potential candidate for the construction of electrochemical sensors for the determination of L-Dopamine.

#### ACKNOWLEDGEMENTS

The authors are grateful for Fundação de Amparo à Pesquisa do Estado de São Paulo (FAPESP - Procs. 2012/11306-0; 2012/05438-1 and 2013/08495-9).

#### Reference

1. R. H. Baney, M. Itoh, A. Sakakibara, T. Suzukit, *Chem. Rev.*, 95 (1995) 1409.
2. S. W. Kuo, F. C. Chang, *Prog. Polym. Sci.*, 36 (2011) 1649.
3. D. Gnanasekaran, K. Madhavan, B. S. R. Reddy, *J. Sci. Ind. Res.*, 68 (2009) 437.
4. D. B. Cordes, P. D. Lickiss, F. Rataboul, *Chem. Rev.*, 110 (2010) 2081.
5. D. Xu, L. S. Loo, K. Wang, *J. Appl. Polym. Sci.*, 122 (2011) 427.
6. C. Ni, G. Ni, L. Zhang, J. Mi, B. Yao, C. Zhu, *J. Coll. Int. Sci.*, 362 (2011) 94.
7. T. A. Tereshchenko, *Polym. Sci.*, 50 (2008) 249.
8. A. Provatas, M. Luft, J. C. Mu, A. H. White, J. G. Matison, B. W. Skelton, *J. Organomet. Chem.*, 565 (1998) 159.
9. E. A. Quadrelli, J. M. Basset, *Coord. Chem. Rev.*, 254 (2010) 707.
10. X. Zhang, J. Sun, S. Fang, X. Han, Y. Li, C. Zhang, *J. Appl. Polym. Sci.*, 122 (2011) 296.
11. M. Handke, A. Kowalewska, *Spectrochim. Acta, Part A: Mol. Biomol. Spectros.*, 79 (2011) 749.
12. S. Gabriel Junior, Preparação, caracterização e aplicações eletroanalíticas de silsesquioxanos e dendrímeros modificados suportados na superfície da sílica gel. Dissertação (Mestrado) – Faculdade de Engenharia, Universidade Estadual Paulista “Júlio de Mesquita Filho”, Ilha Solteira (2010).
13. L. A. Soares, T. F. S. Da Silveira, D. R. Silvestrini, U. O. Bicalho, D. R. Do Carmo, *Int. J. Chem.*, 5 (2013) 39.
14. D. R. Do Carmo, L. L. Paim, *Mater. Res.*, 16 (2013) 164.
15. N. L. Dias Filho, R. M. Costa, M. S. Schultz, *Inorg. Chim. Acta*, 361 (2008) 2314.
16. G. Li, L. Wang, H. Ni, C. U. Pittman Junior, *J. Organomet. Chem.*, 11 (2001) 123.
17. L. A. Soares, Propriedades Analíticas e Eletroanalíticas de um Silsesquioxano Nanoestruturado

- Organofuncionalizado. Dissertação (Mestrado) – Faculdade de Engenharia, Universidade Estadual Paulista “Júlio de Mesquita Filho”, Ilha Solteira (2011).
18. M. Joshi; B. S. Butola; *J. Macromol. Sci. Part C Polym. Rev.*, 44 (2004) 389.
  19. I. Nischang; O. Bruggemann, I. Teasdale, *Angew. Chem. Int. Ed.*, 50 (2011) 4592.
  20. A. Castaldo; G. Quercia-DiFrancia; A. Cassinese; P. D’Angelo, *J. Appl. Phys.*, 103 (2008) 054511.
  21. R. M. Laine, M. F. Roll, *Macromolecules*, 44 (2011) 1073.
  22. H. C. L. Abbenhuis, *Chem. Eur. J.*, 6 (2000) 25.
  23. A. Fina, D. Tabuani, F. Carniato, A. Frache, E. Boccaleri, G. Camino, *Thermochim. Acta*, 440 (2006) 36.
  24. T. F. S. Da Silveira, D. R. Silvestrini, U. O. Bicalho, D. R. Do Carmo, *Int. J. Electrochem. Sci.*, 8 (2013) 872.
  25. D. R. Do Carmo, L. L. Paim, D. R. Silvestrini, A. C. De Sá, U. O. Bicalho, N. R. Stradiotto, *Int. J. Electrochem. Sci.*, 6 (2011) 1175.
  26. M. Morán, C. M. Casado, I. Cuadrado, *Organometallics*, 12 (1993) 4327.
  27. H. W. Ro, E. S. Park, C. L. Soles, D. Y. Yoon, *Chem. Mater.*, 22 (2010) 1330.
  28. H. B. He; B. Li; J. P. Dong; Y. Y. Lei; T. L. Wang; Q. W. Yu; Y. Q. Feng; Y. B. Sun, *ACS Appl. Mater. Interfaces*, 5 (2013) 8058.
  29. M. Bhagiyalaksmi; R. Anuradha; S. Do Park; H. T. Jang, *Micropor. Mesopor. Mater.*, 131 (2010) 265.
  30. E. Devaux, M. Rochery, S. Bourbigot, *Fire Mater.*, 26 (2002) 149.
  31. D. A. Wann, R. J. Less, F. Rataboul, P. D. McCaffrey, A. M. Reilly, H. E. Robertson, P. D. Lickiss, D. W. H. Rankin, *Organometallics*, 27 (2008) 4183.
  32. J. Chojnowski, W. Fortuniak, P. Rościszewski, W. Werel, J. Łukasiak, W. Kamysz, R. Hałasa, *J. Inorg. Organomet. Polym. Mater.*, 16 (2006) 219.
  33. M. Yao; J. Wang; X. Gu; L. Feng, *Progress Chem.*, 24 (2012) 405.
  34. D. M. L. Goodgame; S. Kealey; P. D. Lickiss; A. J. P. White, *J. Mol. Struct.*, 890 (2008) 232.
  35. E. Andrzejewska; A. Marcinkowska; D. Prządka; A. Klozinski; P. Jakubowska, *Polimery*, 58 (2013) 794.
  36. K. Tanaka; Y. Chujo, *Polym. J.*, 45 (2013) 247.
  37. R. M. Laine; M. F. Roll, *Macromolecules*, 44 (2011) 1073.
  38. E. A. Quadrelli; J. M. Basset, *Coord. Chem. Rev.*, 254 (2010) 707.
  39. Z. Kaigiang; L. Bo; Z. Yunhui; L. Hui; Y. Xiaoyan, *Progress Chem.*, 26 (2014) 394.
  40. D. R. Do Carmo, L. L. Paim, N. R. Stradiotto, *Mater. Res. Bull.* 47 (2012) 1028.
  41. L. A. Soares, T. F. S. Da Silveira, D. R. Silvestrini, U. O. Bicalho, N. L. Dias Filho, D. R. Do Carmo, *Int. J. Electrochem. Sci.*, 8 (2013) 4654.
  42. V. V. S. Eswara Dutt; H. A. Mottola, *Anal Chem.*, 46 (1974) 1777.
  43. B. Marciniak; M. Dutkiewicz; H. Marciejewski; M. Kubicki, *Organometallics*, 27 (2008) 793.
  44. D. R. Do Carmo; L. L. Paim; N. L. Dias Filho; N. R. Stradiotto, *App. Surf. Sci.*, 253 (2007) 3683.
  45. J. Coates, Interpretation of Infrared Spectra, A Practical Approach. In Encyclopedia of Analytical Chemistry. John Wiley & Sons LTD, Inc.: Chichester, 2000.
  46. K. Nakamoto, Infrared and raman spectra of inorganic and coordination compounds. New York: John Wiley, p. 484, 1986.
  47. C. W. Ng; J. Ding; Y. Shi; L. M. Gan, *J. Phys. Chem. Solids*, 62 (2001) 767.
  48. D. Engel; E. W. Grabner; *Berichte der Bunsengesellschaft für physikalische Chemie*, 89 (1985) 982.
  49. M. A. Maliki, P. J. Kulesza, *Electroanalysis*, 6 (1996) 113.
  50. S. S. Narayanan, F. Scholz, *Electroanalysis*, 11 (1999) 465.
  51. A. J. Bard; L. R. Faulkner, Electrochemical methods: fundamentals and applications. John Wiley & Sons, Inc.: New York, 2001.
  52. D. Jayasri; S. Narayanan, *Sens. Actuators B*, 119 (2006) 135.

53. M. H. Pournaghi-Azar; H. Nahalparvari, *J. Electroanal. Chem.*, 583 (2005) 307.
54. R. Ojani; J. B. Raoof; B. Norouzi; *Electroanalysis*, 20 (2008) 1996.
55. E. Laviron; *J. Electroanal. Chem.*, 101 (1979) 19.
56. L. A. Soares; W. Yingzi; T. F. S. Silveira; D. R. Silvestrini; U. O. Bicalho; N. L. Dias Filho; D. R. Carmo, *Int. J. Electrochem. Sci.*, 8 (2013) 7565.
57. S. M. Chen; K. T. Peng, *J. Electroanal. Chem.*, 547 (2003) 179.
58. D. K. Maity; H. Mohan; J. P. Mittal, *J. Chem. Soc.*, 4 (1994) 919.
59. M. J. LaVoie; T. G. Hastings, *J. Neurosci.*, 19 (1999) 1484.

© 2015 The Authors. Published by ESG ([www.electrochemsci.org](http://www.electrochemsci.org)). This article is an open access article distributed under the terms and conditions of the Creative Commons Attribution license (<http://creativecommons.org/licenses/by/4.0/>).